Evaluating the Stability of SfM for Digital Surface Model Generation: An Analysis and a Framework

Jesse Sprague
December 21, 2017

Abstract

Traditional photogrammetry is developing into a digital parallel that is less restricted by imaging requirements. The results of this digital revolution are high quality, spatially dense, colorized 3D point clouds. SfM-MVS is a new paradigm in the geosciences and represents a significant advancement in photogrammetry, surveying, and spatial modeling capabilities. Geomorphological processes including erosion, chemical and physical weathering, ecological condition and influence, and natural disasters shape the surface of the Earth. Modeling these phenomena in 3D provides a valuable opportunity for understanding environmental processes. Remote sensing data have become a major source for change detection studies because of their high-temporal resolution, digital format suitable for image processing, synoptic view, and wider selection of spatial and spectral resolution

Error propagation in photogrammetric 3D scene reconstruction techniques has a direct effect on the ability of change detection techniques to accurately quantify change. The current methods for creating accurately geo-located models are by surveying ground control and introducing this point data into the reconstruction process, or by providing a high accuracy, and high precision photocenter location through the use of RTK or ppK geotags in the imagery used for the SfM-MVS process.

Initial concepts that GCP based correction provided a more accurate model for change detection might not be the case. In the context of accurately evaluating change, the ppK/RTK methods for spatially constraining a 3D model might perform better than introducing survey data. The initial reported accuracies for each DEM where within the demonstrated range of high spatial accuracies relevant to the rasters for which they were calculated. Varying the introduced GCPs has a definite effect on the rasters, and despite the RMSE accuracies suggesting that the rasters are accurate, the evaluation of change could be significantly affected if the introduced GCPs are not consistent. In the situation where the GCPs are effected by the change, i.e., mass wasting following a flood or fire, the change evaluation is less likely to be accurate. It appears that survey data can increase the accuracy of a model relative to the actual physical locations when compared to RTK/ppK data but the ability to repeat the distribution of error might be challenged if a GCP used initially is no longer available. While introducing survey data might increase the relative accuracy of a spatial data product, an accurate quantification of the change in repeat scene reconstructions might be more achievable when using ppK/RTK tagged imagery in the SfM-MVS process. The unexpected insights from this investigation have spurred a series of questions that will need to be addressed.

Photogrammetry is the art, science, and technology of obtaining reliable information about physical objects and the environment using photographic images and patterns of recorded radiant electromagnetic energy and other phenomena (Derived from the ASPRS definition). A modern implementation of photogrammetric methods is known as Structure from Motion - Multi-View Stereo (SfM-MVS) whereby a scene is digitally reconstructed in 3 dimensions (3D) using overlapping images collected from various viewpoints. The advancements in this process, as it applies to the geosciences and photogrammetry, are derived from advancements in computer vision, a discipline of computer science [1].

SfM-MVS is a new paradigm in the geosciences and represents a significant advancement in photogrammetry, surveying, and spatial modeling capabilities [2]. The SfM-MVS sequence produces a spatially accurate, colorized 3D point cloud, that can also be georeferenced if given the requisite input information. This is a unique dataset; traditional photogrammetry produces a 2D color image, and LiDAR produces a non-colorized 3D point cloud. Traditional photogrammetry is developing into a digital parallel that is less restricted by imaging requirements. The results of this digital revolution are high quality, spatially dense 3D point clouds.

Geomorphological processes including erosion, chemical and physical weathering, ecological condition and influence, and natural disasters shape the surface of the Earth. Modeling these phenomena in 3D provides a valuable opportunity for understanding environmental processes [3]–[10].

Financial and methodological constraints on traditional techniques for collecting spatial data -- such as photogrammetry, traditional topographic surveys, differential GPS surveys, LiDAR scanning, laser scanning, and total station surveys -- prevent wide scale collection of new 3D datasets [2]. SfM-MVS has an advantage over these traditional methods in both cost and ease of data collection [11]. This advantage has caused a widespread proliferation of the use of SfM-MVS in the geosciences by personnel who are not necessarily experienced in photogrammetry or remote sensing [8]. The SfM-MVS process is often contained in a software package acting as a black box of algorithms. Error propagation within the implementations of these algorithms is not well defined across available commercial or open source options. This combination of novel technology and unknown effects of accuracy introduces potentially un-acknowledged errors as well as capability and application roadblocks.

Physical environmental conditions as well as the physical nature of the subject matter will affect the accuracy of the SfM-MVS products. Some well documented challenges in the SfM-MVS workflow involve texture and color contrast of the subject matter, lighting conditions, orientation of the image set, and the camera used to collect the imagery [12]–[15]. Because the SfM workflow looks for feature correspondence between images, if the features move relative to each other between sequential image captures, the least squares regression cannot resolve the position of the keypoint that has been identified across the images. This problem is encountered frequently when the images contain tree canopies or water bodies. A slight breeze can cause tree canopies to move enough such that the tops of trees fall completely out of the model. Running water or movement on the surface of water bodies also causes holes in the point cloud [12], [16].

High numbers of images can quickly require computational architectures beyond a traditional workstation's capabilities, even high-end processing-oriented servers, to produce a 3D point cloud in a timely fashion [17], [18]. Datasets containing greater than 500 images of high spatial resolution

imagery can take a very long time to process. Spatially accurate 3D models have a very high use value but the time required to generate them is a substantial limiting factor in the potential applications [19]–[23]. Time sensitive decisions in disaster response, defense intelligence, and infrastructure management applications would benefit if spatial data was available within the critical response window [24].

RPAmSS Project

This collaboration project between the Department of Geoinformation and Environmental Technologies at Carinthia University of Applied Sciences (CUAS) in Austria and the Department of Geography at the University of New Mexico in the USA has a specific photogrammetrically oriented research focus linked to the RPAmSS ("New Environmental Robotic Services with a **R**emotely **P**iloted **A**ircraft **m**ulti **S**ensor **S**ystem for Environmental Monitoring") project at CUAS. RPAmSS has been funded by Austrian Research Promotion Agency (FFG) within the 7th call of the COIN - Cooperation and Networks funding line. This cooperative R&D project has the major goal to develop, apply and quantitatively assess the capabilities of a civil, low-cost unmanned aerial multi-sensor system for the fast and high-resolution capture of multidimensional environmental data. In this project, the capabilities of a holistic Remotely Piloted Aircraft multi Sensor System (RPAmSS) for long term monitoring of dynamic river environments and weather phenomena were investigated. Another important focus is the development of new and innovative services based on high quality validated multidimensional RPAS data on demand for long-term monitoring and change detection.

Unmanned Aerial System Platform BRAMOR ppK

We use the professional fixed-wing BRAMOR ppK (**p**ost **p**rocessing **k**inematic) UAS of the Slovenian UAS manufacturer C-Astral platform for high resolution data capture for this research. The UAS has an endurance of up to 3 hours and is equipped with the high-quality autopilot system Kestrel manufactured by Lockheed Martin. Mission planning is done by C-Astral's flight planning software Geopilot. Sensor is a Sony Alpha 6000 (25 MP) RGB camera which is triggered by the autopilot distance based as defined in the mission plan with a 70% image overlap in flight direction and also a 70% overlap between the flight lines. Positional accuracy was improved in a post processing correction procedure within Geopilot software using BRAMOR log file together with RINEX reference data provided on a commercial basis by the Austrian Positioning Service APOS.

Figure 1: Bramor ppK sUAS in Carinthia, Austria.

Technical Details of the BRAMOR ppK UAS are:

Dimensions
Wingspan: 230 cm
Length: 96 cm
Central module length: 67 cm
T/O Weight: 4.7 kg

Features
100% Autonomous
Automatic parachute landing
Orography capable flight planning with GSD maintenance over slopes, hills and valleys
Safe catapult launch
Wind resistance: up to 55 km/h
Compatible with RINEX Base data

ppX Specifications
UAV location accuracy down to 0.6 cm
Onboard survey grade L1&L2 GNSS receiver
GPS, Glonass, Beidou, Galileo ready

Project Test Site – Gail LIFE Nature Conservation project

In recent years different EU-funded LIFE projects have been performed by the Austrian Federal Ministry of Agriculture, Forestry, Environment and Water Management in NATURA 2000 protected sites at the rivers Gail and Drau. Those project sites are not only of importance in the sense of the Habitats Directive but additionally have a relevance for the Birds Directive as migratory birds use the areas for resting. In addition, the Water Framework Directive can be applied to those project areas because they include dynamic rivers. Being surrounded by agricultural fields these LIFE project sites cover all of the four presented legal regulations that ask for monitoring in the EU and demonstrate comparability as both of them have the same legal characteristics. Therefore, the LIFE project site at the river Gail was chosen as study site in the present project. In the following its natural characteristics are described in detail.

The selected project site is the area of the Gail LIFE Nature Conservation project performed by the Austrian BMLFUW. Simultaneously this project site is accounted for an important NATURA 2000 site in Carinthia. The test area is located in the Gailtal east of Hermagor and in between Pressegger See and Nötsch in Carinthia. The project site has a total area of 83 ha and is located at an altitude of 580-600 m above the Adriatic Sea. The directly adjacent floodplain areas are represented by calcareous, sandy and silty soils and loamy and sandy soils while the soils far away from the river Gail are predominantly formed as fen soils rich in humus and lime-free transitional peat bogs. The river Gail traverses the project site as potentially meandering and braided river. In the project site the river is regulated with a trapezoidal- or duplicate trapezoidal profile. Through the reduction of the outflow's cross-sectional area the discharge capacity gets restricted and therewith the danger of flooding caused by the bursting of the dam increases. The fauna of the project site is comparatively well explored and with an amount of at least 35 species with high conservation value after the Habitats Directive the NATURA 2000 site is one of the most important protected areas in Carinthia. Additionally, the project site is used by migratory birds as a resting place and therewith reaches supra-regional significance.

Economic Relevance

The rapid proliferation of UAS, particularly SUAS, and their growing use for mapping and monitoring of a variety of phenomena is putting change detection at the front of the 'art of the possible'. sUAS enable the deployment of large numbers of sensors. Coupled with the collection of hyper-spatial resolution imagery, the growing use of SUAS for mapping and monitoring has resulted in a data flood that requires an understanding of the error propagation inherent in the SfM-MVS process. Automated techniques (e.g., SfM-MVS and automated change detection) for converting collected image data into high level information products, useful for decision support, has the potential to be extremely valuable

if the reliability of these change detection products was known. As the use of sUAS for monitoring a wide variety of phenomena (e.g., pipelines, roads, environmental condition, agriculture, critical infrastructure) expands, so too will the need for rapid, automated generation of high-level information products that characterize 3D shape and detect spatiotemporal change. This requires rapid processing for 3D feature extraction, change detection, and delivery of change intelligence products to a central monitoring station.

The number of SUAS in operation is projected to increase by an order of magnitude or more by the U.S. Department of Transportation (USDOT), the Federal Aviation Administration (FAA), and by market analysis companies in the private industry. The agricultural SUAS market alone is expected to grow from $673M to $2.9B between 2015 and 2021, according to Zion Research [25]. The report notes that the growing reliance on automation to increase efficiency, mitigate labor costs, and produce analyses that result in greater yields, have all drawn farmers to this technology. As airspace restrictions on sUAS loosen, industry, government, and defense organizations will begin to adopt SUAS for myriad mapping and monitoring applications including hazard response, critical infrastructure (e.g., pipelines, electric grid, roadways) monitoring, and time-sensitive science applications. As SUAS use proliferates, the applications will require automated processing routines like change detection from SfM-MVS products, and they will need them to be rapidly and readily available for integration into decision support systems.

SfM-MVS

SfM-MVS is a computer vision technique built on photogrammetric theory whereby the 3D geometry of a scene is reconstructed using redundant 2D imagery. When a scene is viewed from different perspectives, the relative change in position of 3D objects is directly constrained by the change in position of the imaging sensor. By identifying features known as keypoints, then matching these features across images, we can create a set of tielines whose lengths change covariantly with the changes in camera position, and are a function of the 3D structure of the scene being imaged [26].

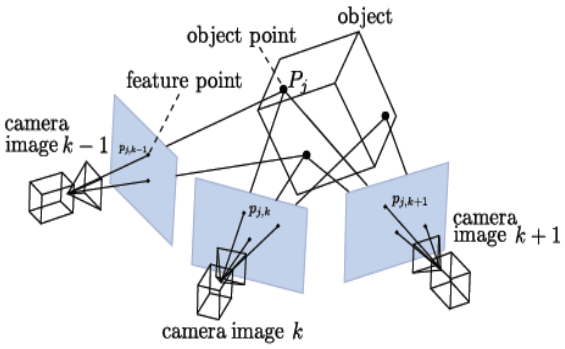

Figure 2: SfM works because the relative position of 3D features changes reliably with a change in viewer perspective.

The creation of a spatially accurate dense point cloud representation of a physical scene can be broken into 9 steps.

1. Extract features in the images [27]
2. Pairwise matching to calculate the fundamental matrix [23]
3. Select and verify the initial pair of images [28]
4. Triangulation of 3D points from initial pair
5. Bundle Adjustment to reduce error of 3D points [29]
6. Add image initial pair, triangulate and store new points to the model
7. Repeat Bundle Adjustment every few images
8. Repeat steps 6 and 7 until entire block has been reconstructed

The result at this point is a sparse point cloud and highly constrained camera positions including x,y,z, and pitch, roll, and yaw information [1], [30].

The MVS step (step 9) follows this process and uses the highly-constrained camera locations and orientations to increase the density of the point cloud by reconstructing the features between the points generated during SfM reconstruction. This is usually accomplished by using several processes (algorithms) that leverage depth maps, convex hulls, and silhouette extraction to densify the sparse point cloud that resulted from the SfM [31].

The result is a colorized point cloud with a density that can exceed those produced by terrestrial laser scanners. SfM-MVS can generate point densities above 10,000 points per square meter given the requisite input imagery resolution and processing parameters [2].

SfM-MVS has an advantage over traditional methods such as traditional photogrammetry, traditional topographic surveys, differential GPS surveys, LiDAR scanning, laser scanning, and total station surveys, in both cost and ease of data collection [11].

SfM in the Geosciences

SfM-MVS is a new paradigm in the geosciences and represents a significant advancement in photogrammetry, surveying, and spatial modeling capabilities [2].

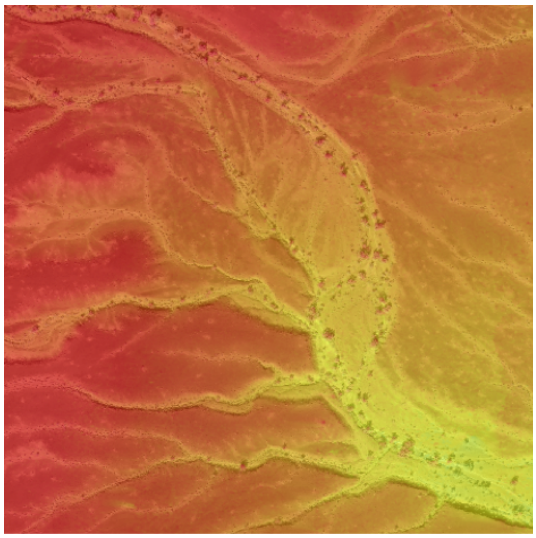

Figure 3: Digital Surface Model or DSM generated using Structure from Motion - Multiview Stereo.

Traditional photogrammetry is developing into a digital parallel that is less restricted by imaging requirements. The results of this digital revolution are high quality, spatially dense, colorized 3D point clouds [32].

Geomorphological processes including erosion, chemical and physical weathering, ecological condition and influence, and natural disasters shape the surface of the Earth. Modeling these phenomena in 3D provides a valuable opportunity for understanding environmental processes [5], [33].

Financial and methodological constraints on traditional techniques for collecting spatial data -- such as photogrammetry, traditional topographic surveys, differential GPS surveys, LiDAR scanning, laser scanning, and total station surveys -- prevent wide scale collection of new 3D datasets [2]. SfM-MVS has an advantage over these traditional methods in both cost and ease of data collection [11].

Physical environmental conditions as well as the physical nature of the subject matter will affect the accuracy of the SfM-MVS products. Some well documented challenges in the SfM-MVS workflow involve texture and color contrast of the subject matter, lighting conditions, orientation of the image set, and the camera used to collect the imagery [12], [13].

Because the SfM work-flow looks for feature correspondence between images, if the features move relative to each other between sequential image captures, the least squares regression cannot resolve the position of the keypoint that has been identified across the images. This problem is encountered frequently when the images contain tree canopies or water bodies. A slight breeze can cause tree canopies to move enough such that the tops of trees fall completely out of the model. Running water or movement on the surface of water bodies also causes holes in the point cloud [16], [34].

SfM-MVS Step by Step

To understand how advancements may be made in the applications of SfM-MVS to the geosciences, we must first understand the workflow. The creation of a spatially accurate point cloud representation of a physical scene can be broken into 9 steps.

Feature Detection

Feature detection starts by identifying common points of features on several different images acquired from different perspectives.

Fundamentally, the challenge is extracting descriptions of points in a way that allows for correct identification and correspondence between these points across a series of images. The goal is to match a point to itself in every photograph that contains it. Early techniques matched image statistics or looked for corners but did not perform well in wide baseline matching [35], [36]. Wide baseline matching requires the use of feature points, or sets of pixels that are invariant to changes in scale and change covariantly with the transformation (affine invariant). Feature types and region detectors are discussed and compared by Mikolajcyk et al. 2005 [37].

One of the most widely used feature type and detectors is the Scale Invariant Feature Transform (SIFT) object recognition system, developed and patented by David Lowe [23], [38], [39]. SIFT is not an ideal photogrammetry solution because it is not fully affine invariant. For photogrammetric purposes, affine invariance is very important because matching happens on relatively planar features under large view changes. Lowe suggests that a combination of SIFT and other feature types be used for best results and will probably be used in future implementations [23]. This was Mikolajcyk's conclusion as well [15].

Improving the feature detection process might be possible. For datasets consisting of a very large number of photos the time required to identify all of the features in each photo is substantial. One possibility to improve this step is to restrict the features to those that have a very high probability of being included in the sparse point cloud and limiting the number of features per photo to an acceptable threshold at which accuracy of the sparse cloud and camera positions is high enough to maintain an accurate dense cloud. Tenting of vertical features in the dense point cloud may be an initial indicator that the sparse cloud was created with too few keypoints per photo.

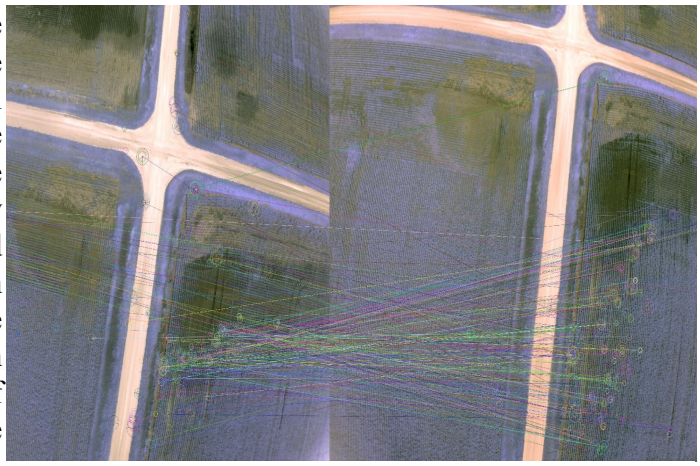

Figure 4: Example of keypoint correspondence between two images of the same content from different perspectives.

Keypoint Correspondence

After keypoints have been located within each image, correspondence between keypoints in different images needs to be determined. One method for this, and the one implemented by SIFT is the approximate nearest neighbor (ANN) method. The distance-ratio criterion has been shown to remove 90% of erroneous matches while discarding less than 5% of correct matches [23]. The number of keypoints is usually very large. *Anecdotally, 240 images have generated about 1.3 billion keypoints when a set of photos is processed using the ultrahigh setting in Agisoft.*

One of the opportunities to expedite the SfM-MVS process is by accelerating the correspondence filter stage. Keypoint descriptors are usually complex, and may be highly dimensional (SIFT produces keypoints with 128 dimensions). One efficient solution has been the k-dimensional trees, or k-d trees. The k-d trees solution is a binary tree algorithm that space-partitions multidimensional data for a nearest neighbor calculation [40]. Anytime data is parsed spatially, many options for accelerating the process arise. One such possibility is the advantage that arises from the modern computing architecture of GPUs. This step in SfM-MVS is well suited to test GPU optimizations.

Keypoint Filtering

To ensure that only correct correspondences remain, a filter is applied to remove erroneous matches. Random sample correspondence (RANSAC), and maximum likelihood sample correspondence (MLESAC) are two methods to filter outliers. Both methods provide robust, fast, and accurate results [41], [42]. MLESAC improves on RANSAC by using a log-likelihood of the fitted solution. The RANSAC process uses the fundamental matrix created by specifying the relationship between two images. Using an 8 (or more) point algorithm [43], the solution to the fundamental matrix constrains the 3D locations of the correctly identified keypoints [44], [45].

Finally, the keypoints that pass the filtering process are organized into tracks or bins. A minimum of two keypoints located in three images is required to make a track. Where the same keypoint occurs twice in an image, the track is considered inconsistent. Maps of consistent tracks are made and the connectivity of the images is known.

Again, advancements in this process have opened the door to grid computing solutions. A promising option is to divide the parameter space into cells. This technique has previously been limited by computing capabilities [30].

Triangulation

During triangulation, the 3D geometry (or structure) of a scene and the different camera poses (i.e. motion) is simultaneously estimated [46]. The feature correspondences found previously are used to construct scene structure and intrinsic and extrinsic parameters of the cameras. Optimizations of this step in projective geometry are a major focus in computer vision fields of study. The methods for reconstructing these parameters are linear algebra problems including matrix multiplication, matrix transformation and Singular Value Decomposition (SVD) [1], [47].

Intrinsic camera parameters are defined by the 3x3 upper triangular matrix k. Additional algorithms correct for shutter type, lense focal length, and other optical distortions. The open source MicMac software incorporates 5 radial distortion corrections, which may be one of the best available. Commercial software is less forthcoming about this but the consensus is MicMac performs very well in this regard [13].

After the camera and scene parameters have been reconstructed, a jointly optimal 3D structure and viewing parameter is produced through a Bundle Adjustment [48]. This process minimizes error in the fitting function. This is done simultaneously with singular value decomposition (SVD). Adjustments to this process can handle scenarios when not all points are visible in all frames. Sequential methods can use smaller computing architectures to process data sets larger than the computer's RAM capacity. These methods are also easily parallelizable and lend themselves more readily to optimization through new computing methods.

When the camera platform is fitted with an RTK GPS, and the photocenter locations are known to within a centimeter of the actual locations, this data can be used to constrain the reconstruction and will result in a model that is geolocated. This is an important advancement, as spatially accurate and geolocated data can be generated without the requirement of setting foot in the area of interest (AOI).

Initial parameter values are derived from an initial pair of images and are used in a non-linear parameter optimization portion of the bundle adjustment. The initial pair should have many matches and a large baseline. Multiple approaches to creating the initial pair exist; options are usually chosen using information available in the metadata found in the EXIF header of the images [1], [45]. The main goal of initialization is to minimize error in the initial pair. This provides an optimality criterion for a nonlinear least squares problem solved using a two-frame bundle adjustment. Bundle adjustment originated from photogrammetry in the 1950s. A bundle refers to the bundle of light rays connecting camera centers to 3D points and adjustment refers to the minimization of the reprojection error [49].

A third camera is added to the scene, and the bundling process is repeated, for any points common to this camera and the existing model. This process continues until every photo has been added to the model and adjusted to fit the parameters. Quadratic or LM algorithms can be used to minimize the cost-functions associated with the optimizations if the computational requirements exceed an acceptable threshold.

The goal is to minimize error across the entire reconstruction. The result is a sparse point cloud representing the subject matter surface and reconstructed camera poses. Most projects will follow this with the MVS processes to generate a dense point cloud of the research area.

Geocorrection and Optimization

After the sparse point cloud is generated, it can be scaled and georeferenced. This is generally done only if the input imagery is not accurately geotagged or if the desired output requires a high degree of geospatial accuracy. With the increasing accuracy of RTK units to geotag photocenters, this step is less often required. Currently, the outputs of RTK informed SFM-MVS products can generate a map with an accuracy of 4cm.

Errors can propagate through the SfM sequence and create non-linear deformations of the final model. Using accurately surveyed ground control in the reconstruction can help constrain the output and a second optimization can be run after tagging features with known, accurate geolocations [2].

Clustering for MVS

The MVS process builds a depth map for each image and merges the separate reconstructions. This allows a high degree of parallelization but contributes to noisy and redundant depth maps. To solve this problem, many of the best-performing (quality-wise) MVS algorithms reconstruct the scene geometry globally [50]. While this method is accurate and clean, the increase in image number rapidly increases the computational expense. Specifically, the RAM requirements will limit the number of images that

can be merged simultaneously. The solution to this problem is to split the images into large chunks. Furukawa 2010 details a preprocessing step known as clustering views for MVS (CMVS), which clusters images into manageable chunks and then runs each chunk individually [32]. The sparse point cloud from SfM is used to produce overlapping image clusters of manageable size such that at least one cluster reconstructs each 3D point. The separate chunks are then aligned into a single dense point cloud.

MVS

Dense point clouds are generated from the MVS process, building upon the sparse point cloud generated from SfM. The goal of MVS is to provide a complete 3D scene reconstruction. Relative to SfM, the point clouds can show at least a two order-of-magnitude increase in point density. There are many versions of the MVS algorithm, there are four main categories into which these algorithms are divided [31].

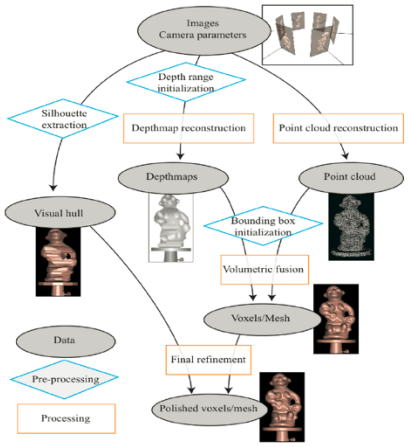

Figure 5: multiple approaches to MVS are demonstrated in this image from Furukawa, et al. 2005.

1. Voxel based methods – based on 3D volume within each voxel grid. These are simple but limited in accuracy by the voxel grid size.
2. Surface evolution-based methods – Deformable polygonal meshes are iteratively evolved to minimize a cost function. Built on hull models, accurate, but difficult for large scenes.
3. Depth map merging methods – compute individual depth maps for each image and merge them. This is the process clustering facilitates, works well in crowded scenes, and avoids the need to resample on a 3D domain.
4. Patch based methods represent scenes with collections of small patches. This method does not require initialization, and is simple and effective. Patched-based MVS (PMVS) has three steps:
    - Match features
    - Expand patches
    - Filter incorrect matches

The MVS image matching algorithms provide point clouds with densities comparable to terrestrial laser scanners (TLS). TLS systems can cost upwards of $200,000 and do not provide color information. MVS point clouds are colorized, creating a product referred to as a photorealistic 3D model.

The SfM-MVS process is derived from computer vision algorithms and has high use value for the geosciences [13], [51], [52]. An evaluation of potential sources of error within the SfM-MVS workflow will contribute to the development of a time sensitive remote sensing technology that has substantially higher use value than the existing available technology.

Ground Control Points Effect on Digital Surface Models

Ground Control affects the accuracy of a DSM resulting from the SfM MVS Process. When evaluating change in geomorphological features like channel shape or profile the placement of these GCPs is

Figure 6: Area in Albuquerque, New Mexico containing the subset of images used for this project.

important. The use of GCPs on the Shoulders, slopes, and toe of the channel have varying levels of control over the resulting DSM Here, 5 different sets of the available GCPs were used to evaluate the difference in the RMSE and the location of resulting difference when toe, slope, or shoulder GCPs are used or withheld [53]. The results include RMSE calculations and difference rasters showing the location of the effect of the GCP choices.

A subset of images from a manned aircraft collection in Albuquerque, New Mexico was used to build 5 independent sparse point clouds. The 'align photos' step in Agisoft PhotoScan is the SfM portion of the SfM-MVS process. Five separate sparse point clouds, or chunks, were created with this align photos step. Then, a unique subset of GCPs were introduced to each chunk during the orthocorrection step prior to the MVS process and subsequent DEM creation.

The first raster constructed used a subset of GCPs containing at least one point in each category. This DEM was considered to be the control against which the other rasters were compared to. This raster was constructed by using GCPs 2, 7, 8, 9, and 10.

The remaining four rasters where generated using different subsets of GCPs as described in the Table 1. Subsequently, the rasters 1 through 4 where subtracted from 0-Control to visually evaluate the variance distribution across the DEMs. Root Mean Square Error (RMSE) was calculated for each raster and is presented in Table 3.

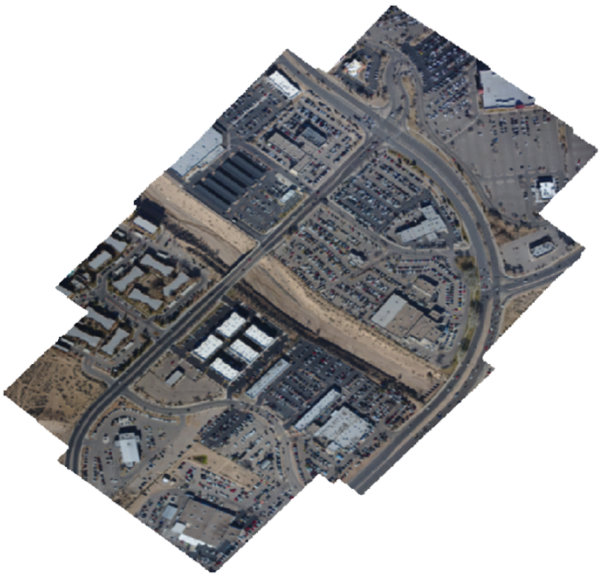

Figure 7: Extent of model constructed using 13 images from manned aircraft in Albuquerque, NM.

Figure 8: GCP Locations used in correction and accuracy evaluation.

Table 1. Control and Check points used for each model.

Raster Number	Name	GCPs used for Correction	GCPs used for RMSE
0	Control	2,7,8,9,10	1,3,4,6
1	No Channel	1,2,6,9,10	3,4,7,8
2	No Slope	1,6,8,10	2,3,4,7,9
3	No Shoulder	2,4,8,9	1,3,6,7,10
4	No Slope or Channel	2,3,4,8,9	1,6,7,10

The initial reported accuracies for each DEM where within the demonstrated range of high spatial accuracies relevant to the rasters for which they were calculated [54]. The lowest (most accurate) horizontal RMSE is 3.1 cm on the control raster, while the highest (least accurate) RMSE calculated is 5.6 cm on the No Shoulder raster. The orthophoto rasters used to calculate these RMSE values have spatial resolutions of 7cm. Vertical accuracies range from 17.5 cm for the No Channel raster to 36.2 cm for the No Shoulder raster. The DEMs used to calculate the vertical RMSEs are all 15cm spatial resolutions.

Table 2: Ground Control Points. This table shows the location and designation information for the ground control used for orthocorrection of the sparse point clouds. GCP number 5 and 11 are withheld altogether, GCP 5 is not visible in the imagery and GCP 11 is only in two of the photos making it insufficient for use.

GCP ID	LAT	LONG	ELEV	Location
1	35.19258793	-106.6592136	1541.676117	Shoulder
2	35.19253269	-106.6592983	1538.972559	Slope
3	35.19237988	-106.6593014	1533.682258	Channel
4	35.19245026	-106.6593665	1534.090158	Channel
5	35.19237649	-106.6597734	1533.876881	N/A
6	35.19219087	-106.6600416	1543.002757	Shoulder
7	35.19203511	-106.6602158	1542.71291	Shoulder
8	35.19267765	-106.6597646	1534.470053	Channel
9	35.19310151	-106.6600477	1539.321839	Slope
10	35.1934887	-106.660303	1544.448501	Shoulder
11	35.19450938	-106.6618758	1541.213749	N/A

Table 3: RMSE Table. Accuracies, as evaluated by the survey control points withheld from each model. Generally, these RMSE values would be accepted as accurate considering the spatial resolution of the raster products they are evaluating.

Summary Table				
RMSE (in Meters)				
Raster Name	Easting	Northing	Horizontal	Elevation
Control	0.022015	0.031178949	0.031178949	0.187513705
No Cannel	0.01719	0.068422999	0.053245857	0.174967603
No Slope	0.0267711	0.037045049	0.049289147	0.177827655
No Shoulder	0.015990569	0.049876161	0.05570369	0.362074449
No Slope or Channel	0.031984	0.012948639	0.045476799	0.222805994

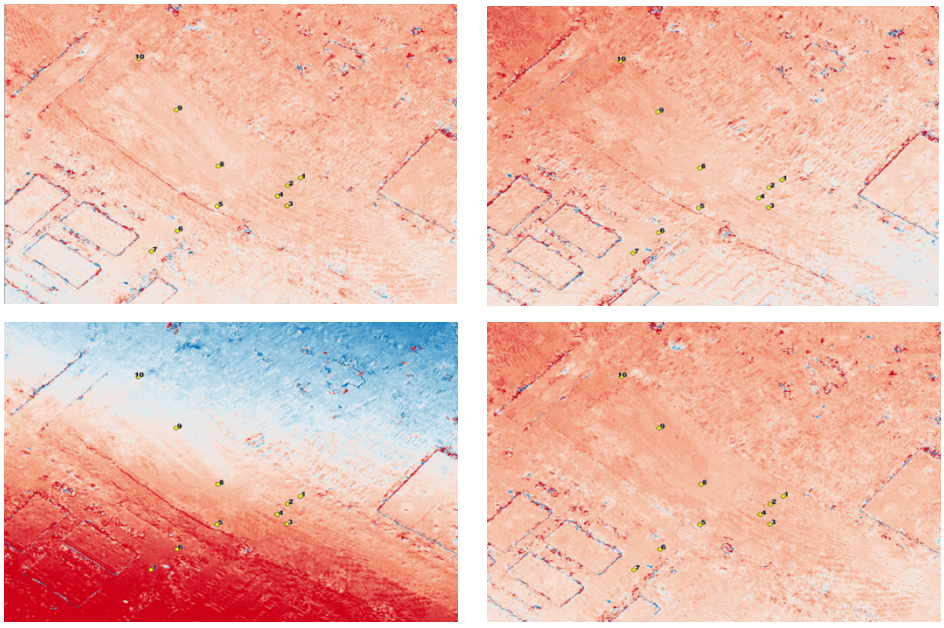

Figure 9: Difference Rasters. These rasters were created by subtracting the control DSM from the rasters 1 through 4. Clockwise from top left: 1, 2, 4, 3.

Difference rasters were generated by subtracting the Control Raster from each of the test rasters. While the immediate vicinity of the GCPs the rasters show a high degree of similarity but the distribution of the differences is visible. Raster 3, No Shoulder, is substantially different from the other rasters but this is most likely caused by the lack of GCPs on the bench, outside of the shoulder region.

Varying the introduced GCPs has a definite effect on the rasters, and despite the RMSE accuracies suggesting that the rasters are accurate, the evaluation of change could be significantly affected if the introduced GCPs are not consistent. In the situation where the GCPs are effected by the change, i.e., mass wasting following a flood or fire, the change evaluation is less likely to be accurate.

Change Detection

In remote sensing applications, changes are considered as surface component alterations with varying rates [55]. Essentially, change detection is the process of identifying differences in the state of an object or phenomenon by observing it at different times, which involves the ability to quantify temporal effects using multi-temporal datasets [56]. Remote sensing data have become a major source for change detection studies because of their high-temporal resolution, digital format suitable for image processing, synoptic view, and wider selection of spatial and spectral resolution [55], [57], [58]. The fundamental framework of change detection is using multi-temporal remote sensing data to qualitatively analyze the temporal effects of phenomenon and quantify the changes [55]. Change detection techniques by using multi-temporal remote sensing data helps in understanding landscape dynamics [59].

Error Propagation

One source of error propagation in the SfM process stems from the non-deterministic techniques used in the generation of the sparse point cloud and camera position estimation. SfM uses MLE, ANN, and RASNAC which will generate slightly different results every time a dataset is processed. The variance of these techniques has not been evaluated in the context of geomorphological change detection and is the focus of this investigation.

Error propagation in the SfM-MVS process directly impacts the ability of these techniques to contribute to understanding change from repeated scene reconstructions over time. Detecting change in

digitally reconstructed models relies on the ability of these models not to show change where there isn't any. Because of the non-deterministic portions of the SfM process, some change will exist even if the exact same imagery is used. By evaluating the variance in SfM when identical inputs are used, it is possible to understand the potential error, and subsequently the potential reliability, of a time series to accurately show change.

Methods for Camera Position Error Propagation Evaluation

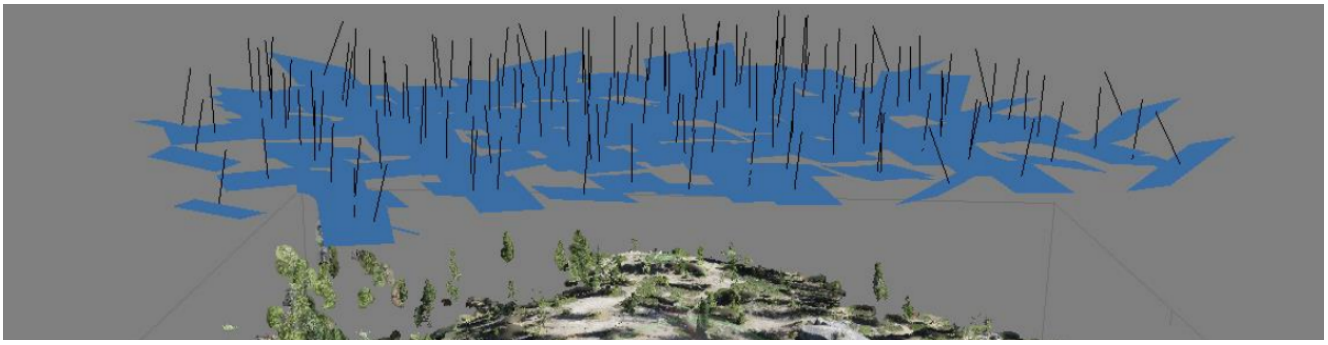

Figure 10: Camera Positions from SfM. Blue planes represent the orthometric position of the camera sensor when the image was collected. Black lines are the normal vector to the sensor and describe the orientation. This investigation examines the consistency of the estimated position and orientation of a set of photos when run through the SfM process multiple times.

Question:
How much variance in estimated camera positions occurs when repeating the SfM process on the exact same set of images?

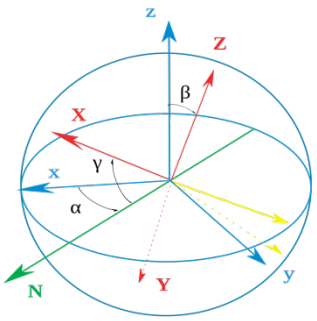

Figure 11: Euler Angles. Six measurements define the position and orientation of an object in 3D space.

Process:
To better understand the error propagation in a digital reconstruction sequence, the SfM step will be evaluated apart from the MVS step, and evaluated for variance in the camera positions that result. Because the camera positions are used in the dense cloud generation, any variance in their estimated locations will contribute to subsequent error in the final 3D product.

To bound the investigation such that the most accurate (i.e., minimum variance) results were achieved, only PPK tagged imagery was used, and every setting in PhotoScan was set to the strictest option.

Jupyter Notebook was used for the data analysis. The Pandas library for Python makes the investigation of iterated results very easy. The python code used to generate the data herein is included as Appendix II.

UAS and GNSS Data:
This project uses aerial imagery collected from an sUAS. Images were collected with a C-Astral Bramor sUAS described above. This imagery is representative of traditional UAS collected methods, using a fixed wing aircraft and a nadir pointing digital camera. The imagery has a ground sample distance of about 1cm. The subject matter of the imagery is a riparian ecosystem and wetlands in Southern Austria. The UAS is outfitted with a PPK GNSS receiver that has provided photocenter locations accurate to 0.06 cm.

CUAS Dataset C-Astral

Austria Dataset C-Astral

- Austria UAS Test Site
    - size (Gb):
    - Number of Input Photos: 15
    - Location:
    - GSD:
    - Sensor:
    - input image number:

Processing Workflow Outline

1. Start new PhotoScan project
2. Run PhotoScan python script
    a. Create new chunk
    b. Load photos
    c. Match and align chunk (SfM)
3. Repeat step two, 30 times
4. Export Camera Positions for each of the 30 Chunks (Manual)

Analysis Workflow Outline

Using a python program to loop the SfM process, 30 point clouds were generated from the same set of input imagery. After this process, the camera position estimation files were exported from the agisoft project. Two runs failed, and were removed from the project. The resulting 28 text files contain the iterated results used in the evaluation of variance. The basic workflow for the portion of work done in the Jupyter Notebook follows:

Step 1

1. Load required python libraries
2. Write the function to parse the text files that PhotoScan exports
3. Write the function to concatenate the results of the parse function into a single dataframe
4. Group dataframe by unique camera (15 groups of 28 runs)
5. Calculate the variance
6. Write the variance dataframe to CSV file for inclusion in this report (Table 1)

Step 2

1. Create 4 DEMs from runs 1 - 4 (Dense Cloud → DEM)
2. Difference DEMs to show variance in rasters

Results

Initial results returned from the iterated processing in Agisoft PhotoScan where so small that the framework of the question had to be re-evaluated. The variance in estimated camera position and orientation constructed by the SfM process is extremely small. The variance in the X position of each photo ranges from a minimum of 0.8 mm to a maximum of 1.0 mm. The variance in the reconstructed Y position ranges from a minimum of 0.02 mm to a maximum of 0.03 mm. The estimated Z values are an order of magnitude smaller ranging from a minimum of 8.1 nanometers to 0.497 micrometers. Both of these values are arbitrarily small such that the Z position can be considered null.

Similarly, the orientation as described by the Euler angles are arbitrarily small, and can probably be held as not varying between runs as well.

Table 4: Variance in estimated positions for each camera. Each value in Table 4 represents the variance contained in 28 values for that particular metric. Each value is smaller than the accuracy of the position information returned from the ppK data by an order of magnitude. These variances suggest that the error propagation in the SfM process is mostly due to other portions of the process. SfM returns almost identical values almost every time.

Variance in Estimated Camera Positions						
28 Iterations on 15 images to evaluate the variance in estimated camera position. Meters and Euler Angles						
Camera Number	X	Y	Z	Omega	Phi	Kappa
0	0.00094300000	0.00002440000	0.00000007530	0.00000220000	0.00000171000	0.00000048800
1	0.00098400000	0.00003140000	0.00000005940	0.00000161000	0.00000029300	0.00000050700
2	0.00097400000	0.00002770000	0.00000002050	0.00000202000	0.00000029100	0.00000049800
3	0.00097300000	0.00002950000	0.00000000810	0.00000179000	0.00000052100	0.00000049400
4	0.00096800000	0.00002910000	0.00000007010	0.00000182000	0.00000096300	0.00000055300
5	0.00089900000	0.00003270000	0.00000027400	0.00000194000	0.00000403000	0.00000047500
6	0.00096000000	0.00003180000	0.00000032400	0.00000169000	0.00000037300	0.00000046600
7	0.00091700000	0.00003160000	0.00000011400	0.00000240000	0.00000136000	0.00000050400
8	0.00096100000	0.00002510000	0.00000023800	0.00000212000	0.00000209000	0.00000047700
9	0.00101000000	0.00003190000	0.00000049700	0.00000103000	0.00000200000	0.00000049200
10	0.00101000000	0.00002980000	0.00000024600	0.00000114000	0.00000179000	0.00000046000
11	0.00101000000	0.00003280000	0.00000010800	0.00000108000	0.00000113000	0.00000043800
12	0.00099900000	0.00003250000	0.00000012700	0.00000115000	0.00000070200	0.00000042100
13	0.00094200000	0.00003330000	0.00000011200	0.00000098700	0.00000056100	0.00000049300
14	0.00093800000	0.00003450000	0.00000007920	0.00000119000	0.00000099700	0.00000055000
Min	0.00089900000	0.00002440000	0.00000000810	0.00000098700	0.00000029100	0.00000042100
Max	0.00101000000	0.00003450000	0.00000049700	0.00000240000	0.00000403000	0.00000055300
Ave	0.00096586667	0.00003054000	0.00000015684	0.00000161113	0.00000125407	0.00000048773

Upon examination of the incredibly small variances in the estimated camera positions, further investigation was warranted into the variance of the resulting rasters. As seen in the previous section, very accurate rasters built from the same imagery may still show internal variances beyond what is considered acceptable. An evaluation of this same types of variances are seen in Figure 12.

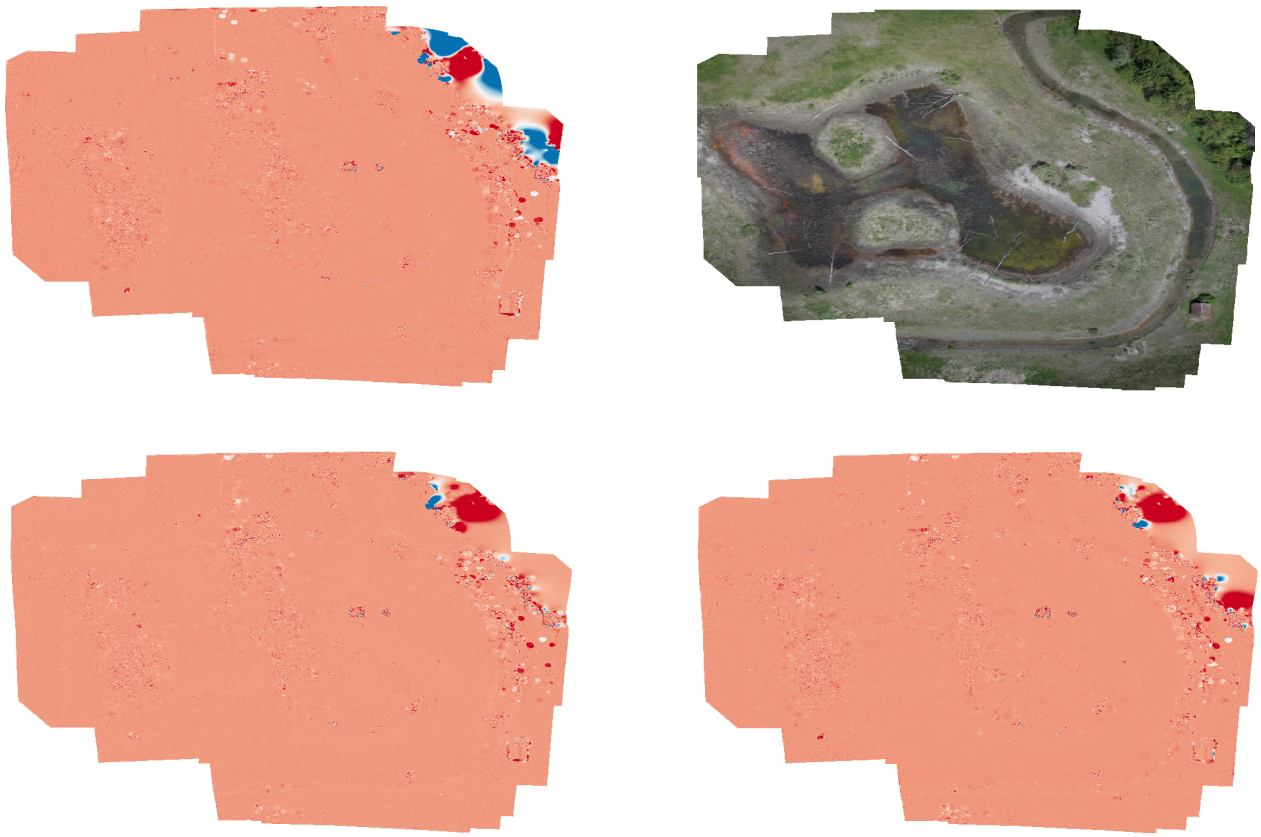

Figure 12: Difference rasters for 4 DSMs that came from the CUAS data. each raster has the same style applied, i.e., the same color represents the same value in all three rasters. The fourth raster is an orthoimage showing the extent of the AOI.

The difference rasters presented in Figure 12 where created by building 4 DEMs from different SfM runs, and subtracting the first one from the remaining three. As seen in Figure 12, the variances are almost non-existent.

The spatial distribution of variance in the brief examination of the DEMs created for the Austria dataset shows that the only variance evident so far is near the edges of the model. The interior portions show almost no difference between each respective run on the same imagery

Figure 13 is an examination of the spatial data products generated from the imagery originating in Austria collected by the Corinthian University of Applied Sciences.

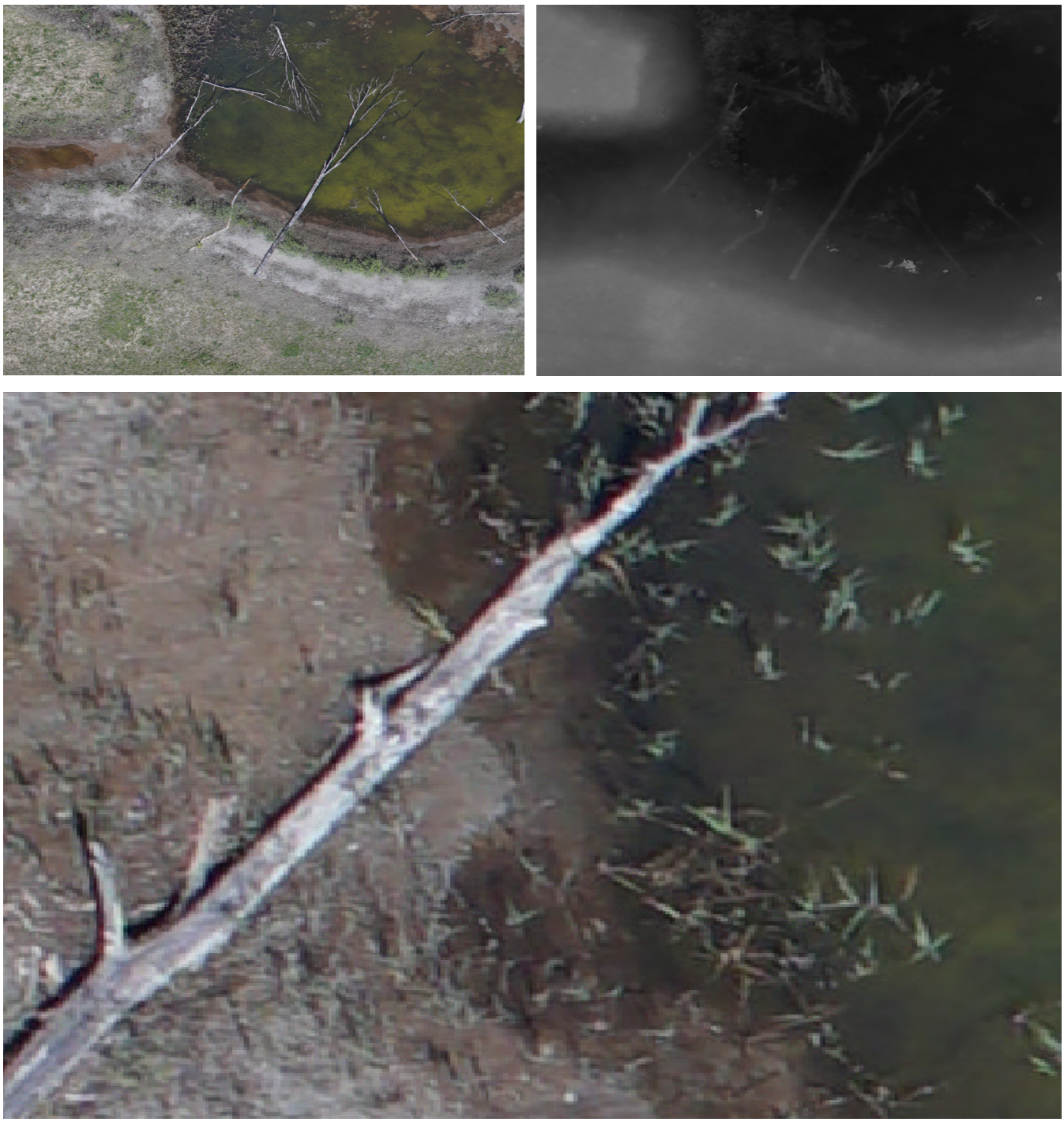

Figure 13: Examples of the orthoimage and DEM created during the repeated processing of the Bramor ppK sUAS in Carinthia, Austria. Top left is a subset of the orthophoto, top right is the DEM, and bottom is a zoomed in view of a portion of the orthophoto in the top left.

Discussion

Error propagation in photogrammetric 3D scene reconstruction techniques has a direct effect on the ability of change detection techniques to accurately quantify change. The current methods for creating accurately geo-located models are by surveying ground control and introducing this point data into the reconstruction process, or by providing a high accuracy, and high precision photocenter location through the use of RTK or ppK geotags in the imagery used for the SfM-MVS process.

Initial concepts that GCP based correction provided a more accurate model for change detection might not be the case. In the context of accurately evaluating change, the ppK/RTK methods for spatially constraining a 3D model might perform better than introducing survey data.

It appears that survey data can increase the accuracy of a model relative to the actual physical locations when compared to RTK/ppK data but the ability to repeat the distribution of error might be challenged if a GCP used initially is no longer available.

While introducing survey data might increase the relative accuracy of a spatial data product, an accurate quantification of the change in repeat scene reconstructions might be more achievable when using ppK/RTK tagged imagery in the SfM-MVS process.

Future Work

The unexpected insights from this investigation have spurred a series of questions that will need to be addressed. Particularly, a more controlled ground survey in a test area where we can collect a repeat data set where controlled volumetric change was generated to simulate erosion or mass movement. A well-controlled experiment of this kind will yield the change detection insights that can answer the question of what method is better performing for accurate change detection, GCP or RTK/ppK.

Lastly, the error propagation in SfM-MVS needs to be evaluated in a non-black-box environment where different parameters can be adjusted and the resultant variance evaluated. One potential method for evaluating the ability of Agisoft PhotoScan to reconstruct models or to evaluate the error propagation in the context of the fact it is a black box would be to repeat the looped iteration of point cloud generation using low, medium, and high settings and compare the variances between these sets of point clouds and camera reconstructions.

Plans to evaluate the utility of point clouds in further context related to neural net and machine learning techniques is also expected. The ability of point clouds to provide multi-dimensional data including shape and color has the potential to increase the ability of object identification when paired with modern processing techniques. The imagery from this research project will be useful in these projects as well. Further change detection related inquiry will benefit from the insight gained during this project. The use of Agisoft PhotoScan for change detection will be further explored by collecting repeat imagery of controlled, inflicted change where geomorphological features can be altered for in-situ controlled volume information to test change detection accuracy from SfM products and techniques.

Bibliography

[1] R. Hartley and A. Zisserman, *Multiple View Geometry in Computer Vision*. Cambridge: Cambridge University Press, 2004.

[2] J. L. Carrivick, M. W. Smith, and D. J. Quincey, *Structure from Motion in the Geosciences*. Chichester, UK: John Wiley & Sons, Ltd, 2016.

[3] D. Jakes, "Process geomorphology, Leo F. Ritter, William C. Brown Company Publishers, Dubuque, Iowa, U.S.A. 1978. No. of pages: 603. Price: U.S. $22.95. ISBN 0 697 05035 1," *Earth Surf. Process.*, vol. 5, no. 2, pp. 203–204, Apr. 1980.

[4] N. Micheletti, J. H. Chandler, and S. N. Lane, "Investigating the geomorphological potential of freely available and accessible structure-from-motion photogrammetry using a smartphone," *Earth Surf. Process. Landforms*, vol. 40, no. 4, pp. 473–486, Mar. 2015.

[5] C. H. Hugenholtz *et al.*, "Geomorphological mapping with a small unmanned aircraft system (sUAS): Feature detection and accuracy assessment of a photogrammetrically-derived digital terrain model," *Geomorphology*, vol. 194, pp. 16–24, Jul. 2013.

[6] M. M. Ouédraogo, A. Degré, C. Debouche, and J. Lisein, "The evaluation of unmanned aerial system-based photogrammetry and terrestrial laser scanning to generate DEMs of agricultural watersheds," *Geomorphology*, vol. 214, pp. 339–355, 2014.

[7] L. Javernick, J. Brasington, and B. Caruso, *Modeling the topography of shallow braided rivers using Structure-from-Motion photogrammetry*, vol. 213. Elsevier B.V., 2014.

[8] M. J. Westoby, J. Brasington, N. F. Glasser, M. J. Hambrey, and J. M. Reynolds, "'Structure-from-Motion' photogrammetry: A low-cost, effective tool for geoscience applications," *Geomorphology*, vol. 179, pp. 300–314, 2012.

[9] F. Clapuyt, V. Vanacker, and K. Van Oost, "Reproducibility of UAV-based earth topography reconstructions based on Structure-from-Motion algorithms," *Geomorphology*, vol. 260, pp. 4–15, 2016.

[10] P. Tarolli, "High-resolution topography for understanding Earth surface processes: Opportunities and challenges," *Geomorphology*, vol. 216. pp. 295–312, 2014.

[11] I. Colomina and P. Molina, "Unmanned aerial systems for photogrammetry and remote sensing: A review," *ISPRS J. Photogramm. Remote Sens.*, vol. 92, pp. 79–97, 2014.

[12] M. A. Fonstad, J. T. Dietrich, B. C. Courville, J. L. Jensen, and P. E. Carbonneau, "Topographic structure from motion: A new development in photogrammetric measurement," *Earth Surf. Process. Landforms*, vol. 38, no. 4, pp. 421–430, 2013.

[13] M. Jaud, S. Passot, R. Le Bivic, C. Delacourt, P. Grandjean, and N. Le Dantec, "Assessing the accuracy of high resolution digital surface models computed by PhotoScan?? and MicMac?? in sub-optimal survey conditions," *Remote Sens.*, vol. 8, no. 6, 2016.

[14] P. Barry and R. Coakley, "Field accuracy test of RPAS photogrammetry," *Int. Arch. Photogramm. Remote Sens. Spat. Inf. Sci. - UAVg2013*, vol. XL-1/W2, pp. 27–31, 2013.

[15] K. Mikolajczyk *et al.*, "A comparison of affine region detectors," *Int. J. Comput. Vis.*, vol. 65, no. 1–2, pp. 43–72, 2005.

[16] L. Wallace, A. Lucieer, Z. Malenovsk???, D. Turner, and P. Vop??nka, "Assessment of forest structure using two UAV techniques: A comparison of airborne laser scanning and structure from motion (SfM) point clouds," *Forests*, vol. 7, no. 3, p. 62, Mar. 2016.

[17] B. Tippetts, D. J. Lee, K. Lillywhite, and J. Archibald, "Review of stereo vision algorithms and their suitability for resource-limited systems," *J. Real-Time Image Process.*, vol. 11, no. 1, pp. 5–25, 2016.

[18] a Irschara and V. Kaufmann, "Towards fully automatic photogrammetric reconstruction using digital images taken from UAVs," *Proc. Int. Soc. Photogramm. Remote Sens.*, vol. XXXVIII, no. October 2015, pp. 65–70, 2010.

[19] H. Kopetz, *Real-Time Systems*. 2011.

[20] H. Kopetz, "Real-Time Systems," *Real-Time Syst.*, p. 338, 2011.

[21] N. D. Molton, A. J. Davison, and I. D. Reid, "Locally Planar Patch Features for Real-Time Structure from Motion," *Bmvc*, p. 90.1-90.10, 2004.

[22] R. Kalarot and J. Morris, "Comparison of FPGA and GPU implementations of real-time stereo vision," *2010 IEEE Comput. Soc. Conf. Comput. Vis. Pattern Recognit. - Work. CVPRW 2010*, pp. 9–15, 2010.

[23] D. G. Lowe, "Distinctive image features from scale invariant keypoints," *Int'l J. Comput. Vis.*, vol. 60, pp. 91–11020042, 2004.

[24] C. D. Lippitt, D. A. Stow, and L. L. Coulter, *Time-Sensitive remote sensing*. New York, NY: Springer New York, 2015.

[25] Zion Research, "Agriculture Drone Market (Fixed Wing, Rotary Blade, Hybrid, Data Management, Imaging Software, and Data Analysis) for Field mapping, Variable Rate Application (VRA), Crop Scouting, Crop Spraying, Livestock, Agriculture Photography and Other Applications:" 2016.

[26] Y. Furukawa and C. Hernández, "Multi-View Stereo: A Tutorial," *Found. Trends® Comput. Graph. Vis.*, vol. 9, no. 1–2, pp. 1–148, 2015.

[27] Y. Sun, L. Zhao, S. Huang, L. Yan, and G. Dissanayake, "L2-SIFT: SIFT feature extraction and matching for large images in large-scale aerial photogrammetry," *ISPRS J. Photogramm. Remote Sens.*, vol. 91, pp. 1–16, 2014.

[28] J. Matas, O. Chum, M. Urban, and T. Pajdla, "Robust wide-baseline stereo from maximally stable extremal regions," *Image Vis. Comput.*, vol. 22, no. 10 SPEC. ISS., pp. 761–767, 2004.

[29] B. Triggs, P. F. McLauchlan, R. I. Hartley, and A. W. Fitzgibbon, "Bundle Adjustment — A Modern Synthesis," in *Vision Algorithms '99*, vol. 34099, 2000, pp. 298–372.

[30] P. H. S. Torr and A. Zisserman, "MLESAC: A New Robust Estimator with Application to Estimating Image Geometry," *Comput. Vis. Image Underst.*, vol. 78, no. 1, pp. 138–156, 2000.

[31] S. M. Seitz, B. Curless, J. Diebel, D. Scharstein, and R. Szeliski, “A Comparison and Evaluation of Multi-View Stereo Reconstruction Algorithms,” *2006 IEEE Comput. Soc. Conf. Comput. Vis. Pattern Recognit. - Vol. 1*, vol. 1, pp. 519–528, 2006.

[32] Y. Furukawa and J. Ponce, “Accurate, dense, and robust multiview stereopsis,” *IEEE Trans. Pattern Anal. Mach. Intell.*, vol. 32, no. 8, pp. 1362–1376, Aug. 2010.

[33] M. W. Smith, J. L. Carrivick, and D. J. Quincey, “Structure from motion photogrammetry in physical geography,” *Prog. Phys. Geogr.*, vol. 40, no. 2, pp. 247–275, 2016.

[34] A. M. Cunliffe, R. E. Brazier, and K. Anderson, “Ultra-fine grain landscape-scale quantification of dryland vegetation structure with drone-acquired structure-from-motion photogrammetry,” *Remote Sens. Environ.*, vol. 183, pp. 129–143, 2016.

[35] A. Baumberg, “Reliable feature matching across widely separated views,” in *Proceedings IEEE Conference on Computer Vision and Pattern Recognition. CVPR 2000 (Cat. No.PR00662)*, 2000, vol. 1, pp. 774–781.

[36] K. Mikolajczyk and C. Schmid, “An Affine Invariant Interest Point Detector,” in *Advanced Information Systems Engineering*, 2002, pp. 128–142.

[37] K. Mikolajczyk and C. Schmid, “A performance evaluation of local descriptors,” *IEEE Trans. Pattern Anal. Mach. Intell.*, vol. 27, no. 10, pp. 1615–1630, 2005.

[38] D. G. Lowe, “Local feature view clustering for 3D object recognition,” *Proc. 2001 IEEE Comput. Soc. Conf. Comput. Vis. Pattern Recognition. CVPR 2001*, vol. 1, p. I-682-I-688, 2001.

[39] D. G. Lowe, “Object recognition from local scale-invariant features,” *Proc. Seventh IEEE Int. Conf. Comput. Vis.*, vol. 2, no. [8, pp. 1150–1157 vol.2, 1999.

[40] J. H. Freidman, J. L. Bentley, and R. A. Finkel, “An Algorithm for Finding Best Matches in Logarithmic Expected Time,” *ACM Trans. Math. Softw.*, vol. 3, no. 3, pp. 209–226, 1977.

[41] M. A. Fischler and R. C. Bolles, “Random sample consensus: a paradigm for model fitting with applications to image analysis and automated cartography,” *Commun. ACM*, vol. 24, no. 6, pp. 381–395, 1981.

[42] S. Choi, T. Kim, and W. Yu, “Performance Evaluation of RANSAC Family,” *Procedings Br. Mach. Vis. Conf. 2009*, p. 81.1-81.12, 2009.

[43] H. C. Longuet-Higgins, “A computer algorithm for reconstructing a scene from two projections,” *Nature*, vol. 293, no. 5828. pp. 133–135, 1981.

[44] R. I. Hartley and F. Kahl, “Global optimization through rotation space search,” *Int. J. Comput. Vis.*, vol. 82, no. 1, pp. 64–79, 2009.

[45] N. Snavely, S. M. Seitz, and R. Szeliski, “Skeletal sets for efficient structure from motion,” *Comput. Vis. Pattern Recognit.*, p. 2, 2008.

[46] S. Ullman, “The Interpretation of Structure from Motion,” *Proc. R. Soc. B Biol. Sci.*, vol. 203, no. 1153, pp. 405–426, Jan. 1979.

[47] N. Snavely, S. M. Seitz, and R. Szeliski, “Modeling the world from Internet photo collections,” *Int. J. Comput. Vis.*, vol. 80, no. 2, pp. 189–210, 2008.

[48] Y. Furukawa and J. Ponce, “Accurate, Dense, and Robust Multi-View Stereopsis,” vol. 1, no. 1, pp. 1–14, 2007.

[49] B. Triggs, P. F. McLauchlan, R. I. Hartley, and A. W. Fitzgibbon, “Bundle Adjustment — A Modern Synthesis,” *Vis. Algorithms Theory Pract.*, vol. 1883, pp. 298–372, 2000.

[50] B. Mi??u????k and J. Ko??eck??, “Piecewise planar city 3D modeling from street view panoramic sequences,” *2009 IEEE Comput. Soc. Conf. Comput. Vis. Pattern Recognit. Work. CVPR Work. 2009*, pp. 2906–2912, 2009.

[51] J. P. Dandois and E. C. Ellis, “High spatial resolution three-dimensional mapping of vegetation spectral dynamics using computer vision,” *Remote Sens. Environ.*, vol. 136, pp. 259–276, 2013.

[52] A. Eltner and D. Schneider, “Analysis of Different Methods for 3D Reconstruction of Natural Surfaces from Parallel-Axes UAV Images,” *Photogramm. Rec.*, vol. 30, no. 151, pp. 279–299, 2015.

[53] M. R. James and S. Robson, “Mitigating systematic error in topographic models derived from UAV and ground-based image networks,” *Earth Surf. Process. Landforms*, vol. 39, no. 10, pp. 1413–1420, 2014.

[54] S. Zhang, C. D. Lippitt, S. M. Bogus, A. C. Loerch, and J. O. Sturm, “The accuracy of aerial triangulation products automatically generated from hyper-spatial resolution digital aerial photography,” *Remote Sens. Lett.*, vol. 7, no. 2, pp. 160–169, 2016.

[55] M. Hussain, D. Chen, A. Cheng, H. Wei, and D. Stanley, “Change {Detection} from {Remotely} {Sensed} {Images}: {From} {Pixel}-based to {Object}-based {Approaches},” *ISPRS J. Photogramm. Remote Sens.*, vol. 80, no. Supplement C, pp. 91–106, Jun. 2013.

[56] A. Singh, “Digital {Change} {Detection} {Techniques} {Using} {Remotely}-sensed {Data},” *Int. J. Remote Sens.*, vol. 10, no. 6, pp. 989–1003, Jun. 1989.

[57] R. S. Lunetta, D. M. Johnson, J. G. Lyon, and J. Crotwell, “Impacts of {Imagery} {Temporal} {Frequency} on {Land}-cover {Change} {Detection} {Monitoring},” *Remote Sens. Environ.*, vol. 89, no. 4, pp. 444–454, Feb. 2004.

[58] N. C. Coops, M. A. Wulder, and J. C. White, *Identifying and {Describing} {Forest} {Disturbance} and {Spatial} {Pattern}: {Data} {Selection} {Issues} and {Methodological} {Implications}*. Boca Raton, FL: CRC Press, 2006.

[59] J. S. Rawat and M. Kumar, “Monitoring {Land} {Use}/{Cover} {Change} {Using} {Remote} {Sensing} and {GIS} {Techniques}: {A} {Case} {Study} of {Hawalbagh} {Block}, {District} {Almora}, {Uttarakhand}, {India},” *Egypt. J. Remote Sens. Sp. Sci.*, vol. 18, no. 1, pp. 77–84, Jun. 2015.